Engineering Mouse Apolipoprotein A-I into a Monomeric, Active Protein Useful for Structural Determination†

Xuefeng Ren,‡ Lei Zhao,‡ Arun Sivashanmugam,‡ Yi Miao,‡ Leslie Korando,‡ Zhengrong Yang,§ Catherine A. Reardon,|| Godfrey S. Getz,|| Christie G. Brouillette,§ W. Gray Jerome,⊥ and Jianjun Wang*,‡

Department of Biochemistry and Molecular Biology, School of Medicine, Wayne State University, Detroit, Michigan 48201, Department of Pathology, University of Chicago, Chicago, Illinois 60637, Center for Biophysical Sciences and Engineering, University of Alabama, Birmingham, Alabama 35294-4400, and Department of Pathology, Vanderbilt University, Medical Center, Nashville, Tennessee 37232-2561

Received May 5, 2005; Revised Manuscript Received August 22, 2005

ABSTRACT: Apolipoprotein AI (apoAI), the major protein component of HDL, is one of the best predictors of coronary artery disease (CAD), with high apoAI and HDL levels being correlated with low occurrences of CAD. The primary function of apoAI is to recruit phospholipid and cholesterol for assembly of HDL particles. Like other exchangeable apolipoproteins, lipid-free apoAI forms a mixture of different oligomers even at 1.0 mg/mL. This self-association property of the exchangeable apolipoproteins is closely associated with the lipoprotein-binding activity of this protein family. It is unclear if the self-association property of apolipoprotein is required for its lipoprotein-binding activity. We developed a novel method for engineering an oligomeric protein to a monomeric, biologically active protein. Using this method, we generated a monomeric mouse apoAI mutant that is active. This mutant contains the first 216 residues of mouse apoAI and replaces six hydrophobic residues with either polar or smaller hydrophobic residues at the defined positions (V118A/A119S/L121Q/T191S/T195S/T199S). Cross-linking results show that this mutant is greater than 90% monomeric at 8 mg/mL. CD, DSC, and NMR results indicate that the mutant maintains an identical secondary, tertiary structure and stability as those of the wild-type mouse apoAI. Lipid-binding assays suggest that the mutant shares an equal lipoprotein-binding activity as that of the wild-type apoAI. In addition, both the monomeric mutant and the wild-type protein make nearly identical rHDL particles. With this monomeric mouse apoAI, high-quality NMR data has been collected, allowing for the NMR structural determination of lipid-free apoAI. On the basis of these results, we conclude that this apoAI mutant is a monomeric, active apoAI useful for structural determination.

Human apoAI[1] is a 243-residue protein that is predicted to form amphipathic α-helices (*1*, *2*). Lipid-free apoAI is water-soluble and tends to self-associate at a low concentration (*3*). In aqueous solutions, the C-terminal domain of apoAI is largely disordered and mainly causes the aggregation of this protein (*4*, *5*). With different extents of lipidation, apoAI forms various HDL subspecies, playing a key role in HDL formation, maturation, and transport. This important role of apoAI depends on its conformational plasticity. At different levels of lipidation, apoAI may exist in one of the four distinct forms, including: (1) lipid-free apoAI; (2) ApoAI on pre-βHDL particles; (3) ApoAI on discoidal HDL particles; and (4) ApoAI on spherical HDL particles (*1*, *6*, *7*). These four different forms dictate four different biological functions of apoAI. However, the conformational switches of apoAI that accompany the transformation among these forms in consequence of lipid environmental changes are unknown due to lack of high-resolution structural data of this protein.

While up to 5−10% of circulating apoAI is lipid-free, the *lipid-free apoAI* seems to be specifically linked to the uptake of cellular phospholipids (*8*). Upon binding to a small amount of phospholipids, apoAI forms pre-βHDL particles, which

† This work was supported by an HDL International Research Award (To J.W.) and RO1 Grants from NIH (HL076620 to J.W., HL49148 to W.G.J. and HL 68661 to G.S.G.). Xuefeng Ren and Arun Sivashanmugam are supported by predoctoral fellowships from the American Heart Association (AHA 0415063Z to X.R. and AHA 0415059Z to A.S.).

* To whom correspondence should be addressed. Dr. Jianjun Wang, Department of Biochemistry and Molecular Biology, School of Medicine, Wayne State University, Detroit, MI 48201. Tel: 313-577-8836. Fax: 313-577-8836. E-mail: jjwang@med.wayne.edu.

‡ Wayne State University.

§ University of Alabama.

|| University of Chicago.

⊥ Vanderbilt University.

[1] Abbreviations: ABCAI, ATP-binding cassette AI transporter; apoE, apolipoprotein E; apoAI, apolipoprotein AI; apoLp-III, apolipophorin III; BS_3, bis(sulfosuccinmidyl)suberate; CAD, coronary artery disease; CD, circular dichroism; CE, cholesterol ester; CETP, cholesterol ester transfer protein; DMPC, dimyristoylphosphatidylcholine; DSC, differential scanning calorimetry; DSS, 2,2-dimethyl-2-silapentane-5-sulfonate; FRET, fluorescence resonance energy transfer; GdnHCl, guanidine hydrochloride; HDL, high-density lipoprotein; rHDL, reconstituted high-density lipoprotein; HSQC, heteronuclear single quantum coherence; IPTG, isopropyl-β-D-thiogalactopyranoside; LCAT, lecithin:cholesterol acyltransferase; LDL, low-density lipoprotein; NMR, nuclear magnetic resonance; PLTP, phospholipid transfer protein; POPC, 1-palmitoyl-2-oleoyl-*sn*-glycero-3-phosphocholine; SDS, sodium dodecyl sulfate; SR-BI, scavenger receptor class B, type I; TROSY, transverse relaxation optimized spectroscopy.

10.1021/bi0508385 CCC: $30.25
Published on Web 10/21/2005

are the most active acceptors of free cholesterol (*7*). Both lipid-free and pre-βHDL apoAI (also called lipid-poor apoAI) activate ABCAI for efficient cholesterol efflux (*9*). Addition of cholesterol to lipid-poor apoAI generates larger and lipid-enriched discoidal HDL. ApoAI on discoidal HDL activates the enzyme, LCAT, that converts free cholesterol into cholesterol ester. This process results in an accumulation of CE in the core of HDL particles and generates spherical HDLs. ApoAI on spherical HDL is able to bind to the HDL receptor, SR-BI, for the selective cholesterol uptaking. ApoAI on different HDL particles also mediates the interactions with two lipid transfer proteins: CETP and PLTP. Together with hepatic lipase, these proteins are involved in regulating the remodeling of HDL in plasma and maintaining a balance between the lipid-free and lipid-bound apoAI (*10*).

The conformational plasticity of apoAI plays a critical role in its multiple biological functions. This is especially true for the phospholipid-binding activity of lipid-free apoAI. Phospholipid binding probably triggers a conformational change of lipid-free apoAI that facilitates the uptake of cholesterol, and this process is the key event that initiates HDL formation in vivo. It is unknown, however, what are the structural features in lipid-free apoAI that regulate such a conformational switch upon binding to phospholipids. High-resolution structure of lipid-free apoAI is thus needed to improve our understanding of these putative apoAI conformational changes. In 1997, a 4.0 Å resolution X-ray crystal structure of an N-terminal deletion mutant of human apoAI, apoAI(44−243), in the absence of lipids was reported and suggested that this structure is a putative "*lipid-bound like*" structure (*11*). It adopts an unusual, extended, amphipathic α-helical open conformation, which is a tetrameric, continuously curved, horseshoe-shaped structure. The crystal was obtained in a buffer of high-salt concentration. A new crystal form of apoAI(44−243) has been reported to possibly adopt a helix-bundle structure, even though no detailed structure has been published at this moment (*12*). Recently, secondary structures of both human apoAI(1−186) and apoAI(1−243) were reported in the presence of SDS using NMR techniques (*13*, *14*). These NMR-derived secondary structures are very similar to the X-ray crystal structure in terms of helix locations; however, no tertiary interactions were observed. Information of the structures of apoAI on HDL particles is lacking. For discoidal HDL particles, the most popular current model is the "double belt" model, which is supported by data using FRET (*15*), mass spectrometry along with cross-linking (*16*), and Fourier transform infrared (PATIR-FTIR) spectroscopy (*17*).

Structural studies of lipid-free apoAI are hindered by the aggregation property of this protein. ApoAI forms a mixture of different oligomers even at 1 mg/mL, making it impossible for NMR spectral analysis and preventing this protein from crystallization under normal conditions. Thus, no structure of full-length apoAI in the lipid-free state is currently available. To determine the structure of lipid-free apoAI, the aggregation tendency of this protein must be overcome. Aggregation is a common property of human exchangeable apolipoproteins which share a common lipid-binding activity. It has been proposed that the lipoprotein-binding activity of apoAI might be correlated with its aggregation tendency. However, there is no experimental evidence supporting this hypothesis. We recently developed a novel strategy for quick identification of the critical residues that are responsible for protein aggregation. This strategy also includes a high throughput method for quickly characterizing the oligomeric states of proteins at high concentrations. Using this strategy, we prepared a monomeric apoE C-terminal domain at 5 mg/mL (*18*), whereas the wild-type apoE C-terminal domain forms a mixture of different oligomers at 1 mg/mL (*19*). Interestingly, our data also demonstrated that this monomeric apoE C-terminal domain displayed an equal lipoprotein-binding activity as that of the wild-type protein (*18*). Using the same mutations, we also prepared a monomeric, biologically active, full-length apoE (manuscript in preparation). This result provides direct experimental evidence that, at least for apoE, the lipoprotein binding is independent of its aggregation property. In this report, we describe this strategy and explain how it is applied to mouse apoAI protein to achieve a monomeric, biologically active apoAI mutant. We have chosen to apply this strategy to mouse apoAI, since even as an intact protein, it has a lower tendency to aggregate than human apoAI (*20*). In addition, we demonstrate that this monomeric apoAI mutant maintains the same secondary and tertiary structures and displays an identical stability to those of the wild-type mouse apoAI protein. More importantly, the monomeric apoAI mutant has the same ability to generate nearly identical rHDL particles with POPC as those particles generated using wild-type mouse apoAI. With this mutant, we have collected high quality NMR data for the structure determination of apoAI in the lipid-free state.

EXPERIMENTAL PROCEDURES

Bacterial High-Level Expression of Mouse ApoAI and Mutants. BamH I and Hind III sites were used for subcloning of mouse apoAI on a pET30a(+) plasmid vector (Novagen). A Factor Xa cleavage site was introduced between the His-tag in the pET30a and the mouse apoAI sequence. With this DNA construct, expression was carried out using *Escherichia coli* BL-21(DE3) cells. The culture was grown in minimal M9 medium (kanamycin, 30 μg/mL) at 37 °C until it reached an OD of 0.8−1.0 at 600 nm. Expression was then induced by IPTG (0.5 mM final), and the culture continued overnight at 20 °C. The cells were harvested by centrifugation. The cell pellet was resuspended in binding buffer (10 mL/g cells, 20 mM Tris-HCl, 500 mM NaCl, 2.5 mM imidazole, and 0.1 mM PMSF at pH 7.9) and sonicated on ice. The pellet was dissolved in 6 M urea and sonicated. All supernatant fractions (2 M urea) were combined and applied on a His·Bind resin column (Novagen). The column was washed with a large amount of binding buffer and then the wash buffer containing 20−40 mM imidazole. The purified recombinant protein was eluted from the column using buffer containing 1.0 M imidazole. The eluted protein was dialyzed against 10 mM ammonium bicarbonate to remove imidazole and then lyophilized. Factor Xa cleavage was carried out at an enzyme/protein ratio of 1:1000 at 0 °C for 48 h at 15 mg/mL protein concentration with slight shaking. We observed a secondary Factor Xa cleavage site in mouse apoAI. Mass spectroscopic data indicated that this secondary cleavage site is an arginine at position 192. To avoid this secondary cleavage, this Arg was mutated to a serine. The mutant, mouse apoAI(R192S), only gave a single factor Xa cleavage site at the desired position as confirmed by mass spectroscopy. The reaction products were subjected to the Xarrest

Agarose (Novagen) to capture the Factor Xa and then reloaded onto the His·Bind resin column to remove the His-tag. The purified protein was then dialyzed against 10 mM ammonium bicarbonate and lyophilized. Using this expression system, we can routinely produce ~100−500 mg/L of purified mouse apoAI and its mutants.

Site-Directed Mutagenesis. Site-directed mutagenesis was carried out using the Quickchange mutagenesis kit from Stratagene (Stratagene, CA). Briefly, primers containing the desired mutations were annealed to the denatured DNA expression vector harboring mouse apoAI gene, which was then extended using PfuTurbo DNA polymerase to generate nicked, circular strands. The methylated, nonmutated parental DNA was digested using Dpn I. The circular, nicked, double-stranded DNA containing the mutation was then transformed into BL-21(DE3) cells. The mutations were confirmed by DNA sequencing.

Cross-Linking Experiments. Lipid-free mouse apoAI (1−10 mg/mL) or lipid-bound apoAI (1 mg/mL) in 50 mM sodium phosphate and 50 mM NaCl at pH 7.2 were incubated for 30 min with BS_3, (Pierce, final concentration 0.5 mM). The reaction mixture was quenched by adding 1 M Tris-HCl and 5× SDS−PAGE sample buffer and then loaded on a 6−12% Tricine/PAGE gel. The populations of different oligomers are estimated using the band intensities of the oligomers as quantified using the software of Kodak Gel Logic 100 Imaging System.

CD Spectroscopy and Stability Measurement. CD measurements were carried out on an AVIV model 62DS CD spectrometer (AVIV Instruments, Inc., Lakewood NJ), with a variable temperature capability under computer control within ±0.2 °C. GdnHCl denaturation was performed as described (*21*) and monitored by CD at 222 nm in a 0.1 cm path length cuvette at 20 °C. Protein concentrations were determined by the Markwell modification of the Lowry protein assay (*22*) and absorbance at 280 nm using a spectrophotometer, which gave a similar result of the protein concentration by both methods. The concentrations of denaturant were determined using the density formulas given by Pace et al. (*21*). The α-helical content in apoAI proteins was calculated from the molar ellipticity at 222 nm, using the mean residue weight of mouse apoAI(1−216)-WT (116.98), apoAI(1−216)-P4/L3 (116.80), and apoAI(1−240) (116.86).

Differential Scanning Calorimetry. All calorimetric scans were performed with an N-DSC II differential scanning calorimeter. Lyophilized protein sample was dissolved in 50 mM sodium phosphate, pH 7.4, with 50 mM sodium chloride and 0.1 mM sodium azide. Buffer was loaded into the DSC cells and scanned from 0 to 110 °C at 1 °C/min several times to establish buffer baseline. Protein solution was degassed and loaded into sample cell at approximately 25 °C. Two up scans with the same protein sample were recorded to determine reversibility. Exact concentration of protein in the cell was determined by absorbance at 280 nm using an extinction coefficient of 34 850 M^{-1} cm^{-1}. DSC data analysis was carried out using MicroCal Origin for DSC software.

NMR Methods. The NMR sample of the monomeric mouse apoAI mutant contained 25 mM sodium phosphate, 25 mM NaCl, 5 mM EDTA, 0.1 mM NaN_3, pH 7.2, and 0.4−1 mM triple-labeled protein in 95% H_2O/5% D_2O. The chemical shift was referenced using DSS. All NMR experiments were performed at 30 °C on a Varian Inova 500 MHz spectrometer equipped with a triple-resonance, *z*-axis gradient probe. The 2D ^1H-^{15}N HSQC collected was a sensitivity-enhanced experiment with 1024 points at the proton dimension and 256 complex points at the ^{15}N dimension. The acquisition times for both dimensions were 64 ms. The NMR data processing was achieved using nmrPipe and nmrDraw software (*23*), and analyzed with PIPP (*24*).

DMPC Binding Assay. Ten milligrams of DMPC (Avanti Polar Lipids Inc., AL) was dissolved in a mixture of chloroform and methanol (3:1 v/v), dried using N_2, and placed under vacuum for at least 10 h. One milliliter of prewarmed buffer was added (10 mM Tris-HCl, pH7.2, 150 mM NaCl, and 0.5 mM EDTA) to a final lipid concentration of 10 mg/mL and vortexed several times, 30 s each. Using a 200 nm filter, unilamellar vesicles (~200 nm in diameter) were prepared by extrusion (*25*). The protein-induced transformation of DMPC vesicles into protein/DMPC discoidal complexes was monitored as a function of time (*26*). Two different ratios of apoAI and DMPC (1:1 and 1:2.5, w/w) were used in this assay. ApoAI/DMPC vesicles in buffer were added into a 1-mL thermostat cuvette and mixed for 5−10 s at 24 °C. The clearance of solution was monitored using a Perkin-Elmer spectrophotometer (model Lambda 3B) at 490 nm. All solutions were preincubated at 24 °C before reaction.

Preparation of rHDL. The rHDL particles were prepared using the sodium cholate dialysis method (*27*, 28) with POPC, mouse apoAI, and cholate in a molar ratio of 80:1:108. POPC was dissolved in $CHCl_3$ and dried under nitrogen, then resuspended in 50 mM sodium phosphate and 50 mM NaCl, pH 7.2. After being vortexed thoroughly, sodium cholate was added into the mixture followed by vortexing for another 3 min. The solution was incubated at 37 °C and vortexed every 15 min until completely clear. Mouse apoAI protein was added, and the protein/lipid mixture was incubated for 1 h at 37 °C. Sodium cholate was removed by bio-bead method (*29*).

Electron Microscopy. The rHDL and DMPC particles were absorbed to hydrophilic, carbon and Formvar-coated grids. Samples were negatively stained for 20 s with 2% phosphotungstic acid, pH7.0. Digital images were taken using a Philips CM-30 electron microscope equipped at 80 keV accelerating voltage. For quantification, at least 10 arbitrarily selected fields were chosen and more than 25 particles per field were measured (>250 particles per condition).

RESULTS

General Description of the Strategy. Figure 1 shows a flowchart, demonstrating the principle of this method. The sequence alignment step (step 1) allows identification of the conserved regions of the protein, potentially providing suggestions of the critical residues that are responsible for aggregation. In this step, several residues are hypothesized to be responsible for aggregation. Experiments are then carried out in the following two steps to test if these residues are indeed responsible for aggregation. In step 2, the hypothesized critical residues are mutated. Usually, 5−10 mutants are prepared to mutate the hypothesized critical residues one at a time, two at a time, or several at a time. In this way, we can localize the residues that are responsible

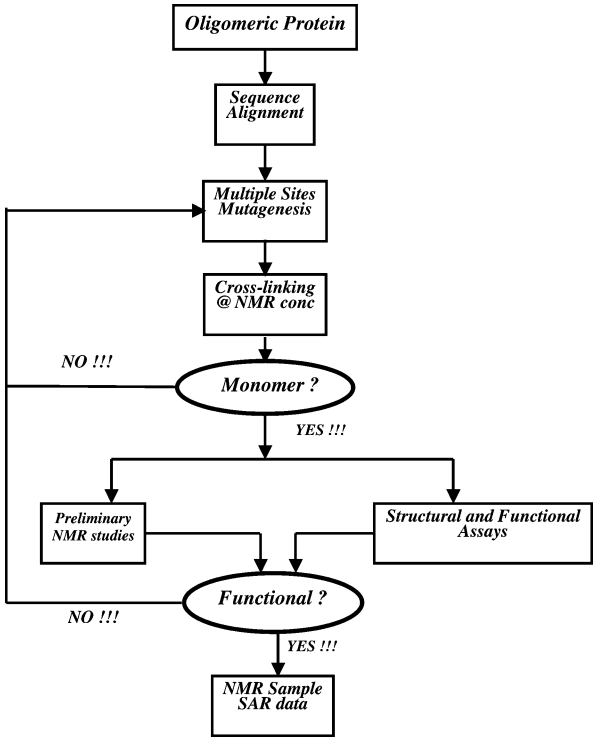

FIGURE 1: A flowchart of the strategy to generate a monomeric, biologically active protein from an oligomeric protein for structural studies.

for aggregation. Once the mutants have been prepared, a method is required for quick characterization of the oligomeric states of mutants. Several different methods, including sedimentation equilibrium, light scattering, NMR relaxation measurements, and cross-linking experiments, can be used. Our results indicated that the cross-linking experiment is the best method for this purpose. Unlike the other measurements, cross-linking is a simple experiment, which essentially includes an incubation of the mutant with cross-linker, followed by a SDS−PAGE. In addition, several mutants can be characterized at the same time (8−16 mutants in a few hours). Finally, cross-linking experiments can be readily carried out at different sample concentrations. This provides an advantage for those proteins, such as apoAI, whose aggregation is concentration-dependent. For NMR samples, we usually carried out cross-linking experiments at 5−25 mg/mL for a protein with a molecular weight of 20−30 kDa. If a monomeric mutant is identified, preliminary CD/NMR experiments are carried out for both the monomeric mutant and the wild-type protein to ensure that the mutations do not alter secondary and tertiary structures of the protein. In addition, several functional assays are carried out for both the monomeric mutant and wild-type protein to assess biological activity. Only the monomeric mutant exhibiting biological activity is considered for further structural determination. If no appropriate monomeric mutant is identified or the monomeric mutant is not biologically active in the first round of mutagenesis, more mutations are designed and prepared. When this method is used, one cycle of engineering usually only takes about 2 weeks.

Application to Mouse ApoAI. We chose mouse apoAI, since this protein aggregates much less than its human counterpart (*20*). It is reported that the C-terminal region of apoAI causes aggregation (*4*); we prepared several C-terminal

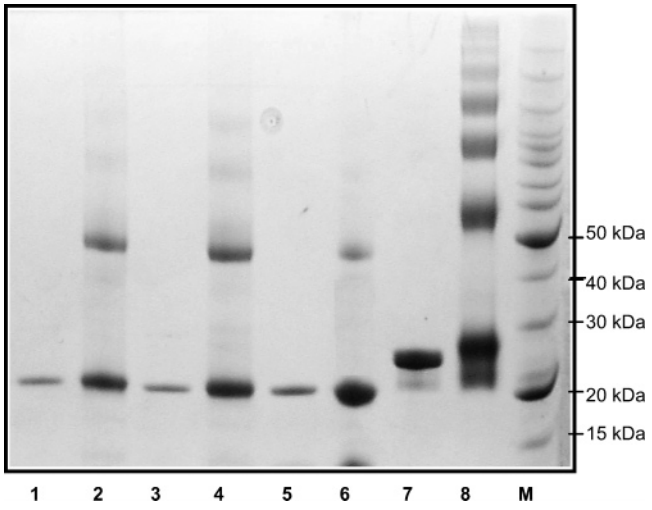

FIGURE 2: Tricine gel (6−12%) of apoAI proteins in 50 mM sodium phosphate saline, pH 7.2. Lanes: 1, apoAI(1−216)-P4, no cross-linking; 2, apoAI(1−216)-P4, cross-linking (7 mg/mL); 3, apoAI(1−216)-WT, no cross-linking; 4, apoAI(1−216)-WT, cross-linking (5 mg/mL); 5, apoAI(1−216)-P4/L3, no cross-linking; 6, apoAI(1−216)-P4/L3, cross-linking (8 mg/mL); 7, human apoAI-(1−243), no cross-linking; 8, human apoAI(1−243), cross-linking (1 mg/mL).

truncation mutants of mouse apoAI, including apoAI(1−206), apoAI(1−216), apoAI(1−229). Cross-linking experiments showed that mouse apoAI(1−206) exhibits ∼50% monomer, 35% dimer, and 15% other oligomers at ∼7 mg/mL, whereas apoAI(1−216) showed a similar population of different oligomers at a lower concentration (5 mg/mL, Figure 2, lane 4). With this result, we started to work on mouse apoAI(1−206) as our starting point. Using the above strategy, we prepared several mutants of mouse apoAI(1−206). The mutant design is based on the fact that lipid-free apoAI forms an amphipathic helix-bundle with hydrophobic and hydrophilic faces. In the helix bundle, the hydrophobic surfaces face each other, whereas the hydrophilic surfaces point to the outside of the bundle. If a hydrophilic surface contains several hydrophobic residues, this helix will not be stable and will likely protect these hydrophobic residues by associating with each other. Using the helix locations shown by Frank and Marcel (*2*) and sequence alignment with human apoAI, we drew helix wheel diagrams for mouse apoAI(1−240) in which the first 43 residues were omitted since they were not present in the X-ray crystal structure (Figure 3). It clearly demonstrated that three hydrophobic Thr residues in helix 8 were located on the hydrophilic surface. We mutated these residues to the more hydrophilic Ser residues (T191S/T195S/T199S, apoAI(1−206)-P4 mutant) and found that this mutant was almost completely monomeric at 6−8 mg/mL (∼95% monomeric).

Another possible reason for apoAI's aggregation is the hydrophobic nature of the loops that connect the helices. For example, residues $L_{63}GPLT_{67}$ form loop 1 that connects helices 1 and 2. This loop contains four hydrophobic residues in a total of five residues. This situation is also seen in residues $V_{118}APL_{121}$, which form loop 3, and in residues L_{140}-$SPVA_{144}$, which form loop 4, as well as in residues L_{162}-APH_{165}, which form loop 5. In contrast to the loops in both apoLp-III and the apoE N-terminal domain, these loops in apoAI are indeed much more hydrophobic. We speculate that the loop hydrophobicity may promote apoAI aggregation via

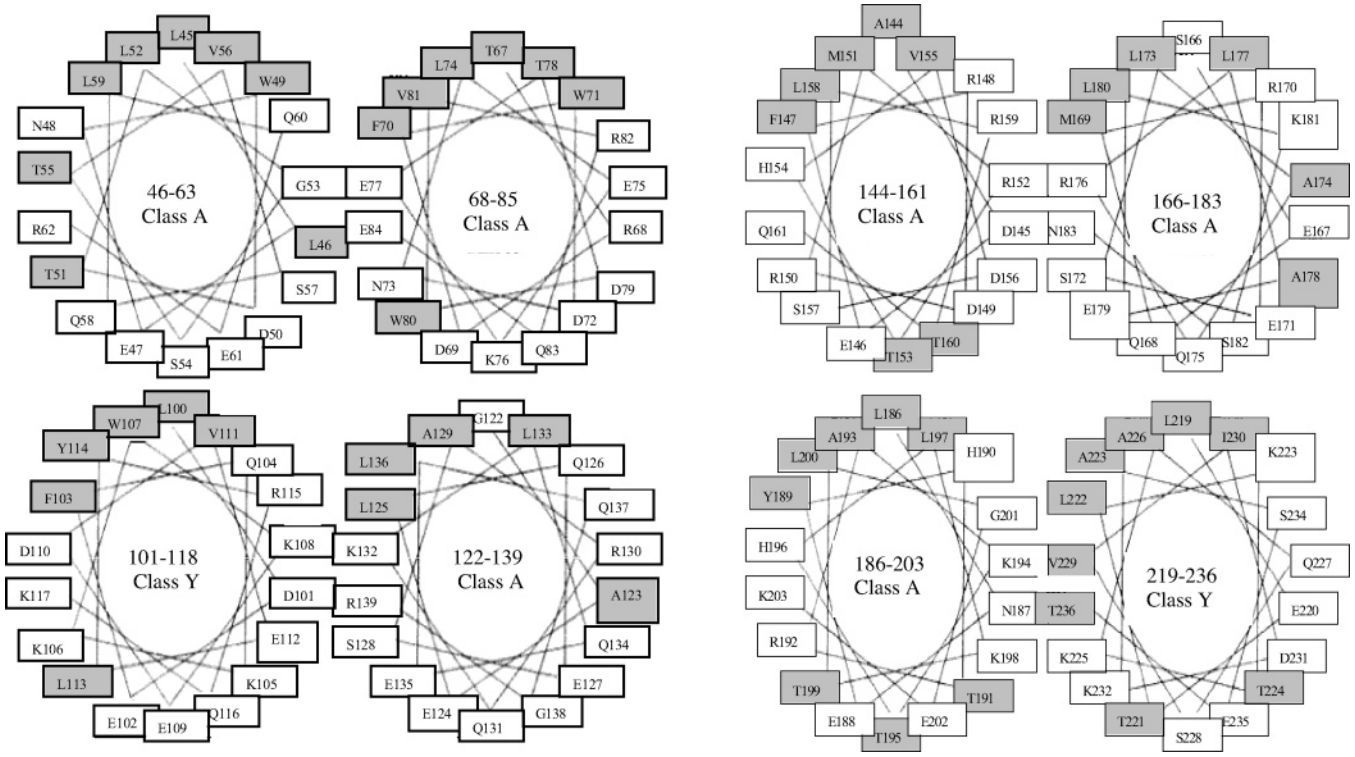

FIGURE 3: Helix wheel diagrams of mouse apoAI. This diagram is generated using sequence homology between human and mouse apoAI. The shaded residues are hydrophobic residues, and open boxes are hydrophilic residues. The first 43-residues are not shown due to the absence of these residues in the X-ray crystal structure.

a head-to-head association, thus, forming a long, rod-shaped, helix-bundle aggregate. Therefore, we further mutated these loop regions with hydrophilic residues in addition to the primary mutations (P4). We found that a mutant, apoAI(1−216)-P4/L3, which contains both mutations of P4 and L3 (loop 3) (V118A/A119S/L121Q/T191S/T195S/T199S), is largely monomeric at 8 mg/mL (Figure 2, lane 6). The other mutations, for example, loop 1 or loop 4, displayed a mixture of oligomers (50% monomer, 40% dimer, and 10% trimer). Similarly, both wild-type apoAI(1−216) (5 mg/mL) and human apoAI(1−243) (1 mg/mL) form a mixture of monomer, dimer, trimer, and other higher oligomers (Figure 2, lanes 4 and 8). We prepared triple-labeled proteins with $^{2}H/^{13}C/^{15}N$ and carried out NMR studies of both the monomeric mouse apoAI(1−216)-P4/L3 and apoAI(1−240). Figure 4 shows TROSY ^{1}H-^{15}N HSQC NMR spectra (5 mg/mL for apoAI(1−240) and 30 mg/mL for apoAI(1−216)-P4/L3). As expected, the monomeric apoAI(1−216)-P4/L3 mutant gives high-quality NMR spectrum with narrower line widths (Figure 4, left panel). In contrast, mouse apoAI(1−240) produces poor-quality HSQC spectrum with broader line widths and many missing cross-peaks (Figure 4, light panel). This result confirms that apoAI(1−240) forms large aggregation, resulting in an overall slower tumbling that produces larger line widths of the spectrum of apoAI(1−240).

Monomeric ApoAI(1−216) Maintains Structural and Stability Integrity of ApoAI. With this monomeric apoAI(1−216), we carried out biophysical studies. Using far-UV and near-UV CD spectroscopy, we show that the monomeric mutant, apoAI(1−216)-P4/L3, and wild-type, apoAI(1−216)-WT, adopt nearly identical secondary and tertiary structures. Figure 5 shows the far-UV CD spectra of these two proteins and full-length wild-type mouse apoAI, demonstrating that both apoAI(1−216) proteins, apoAI(1−216)-P4/L3 and apoAI(1−216)-WT, display an identical CD spectra which is slightly different from the spectrum of apoAI(1−240). The inset shows the near-UV CD spectra of these three proteins, indicating a similar difference between apoAI(1−216) and full-length apoAI. However, overall near-UV CD spectra of all three proteins are similar. This result suggests that both the secondary and tertiary structures of apoAI(1−216) proteins are identical, indicating that the mutations in the monomeric apoAI(1−216)-P4/L3 do not alter the structure of this protein. We noticed that even though the percentages of α-helix of apoAI(1−216)-WT (57.6%) and apoAI(1−216)-P4/L3 (55.5%) are higher than that of apoAI(1−240) (48.6%), the similar numbers of residues (about 120−124 residues) are in the helical region in all three proteins. This suggests that the C-terminal 24-residues of mouse apoAI is largely disordered. The CD result is confirmed by NMR spectroscopy. The ^{1}H-^{15}N HSQC NMR spectra of the full-length mouse apoAI and the monomeric apoAI(1−216) (Figure 4) indicate a nearly identical spectral pattern as highlighted by arrows, suggesting that these two proteins may adopt an identical tertiary structure.

Two techniques were used to characterize the stability of these proteins. First, we carried out DSC experiments. Figure 6 shows the DSC profiles of the monomeric apoAI(1−216) mutant, apoAI(1−216)-WT, and apoAI(1−240) at different concentrations. At a lower concentration (0.67 mg/mL), apoAI(1−216)-WT displays a sharp and symmetric DSC profile. A ratio of close to 1 for the van't Hoff to calorimetric enthalpies, $\Delta H_v/\Delta H_c$, is consistent with the existence of a monomer as the major species in solution. The monomeric apoAI(1−216) mutant displays a similar DSC profile at a much higher concentration (2.8 mg/mL), which is consistent with the cross-linking result. The $\Delta H_v/\Delta H_c$ for apoAI(1−

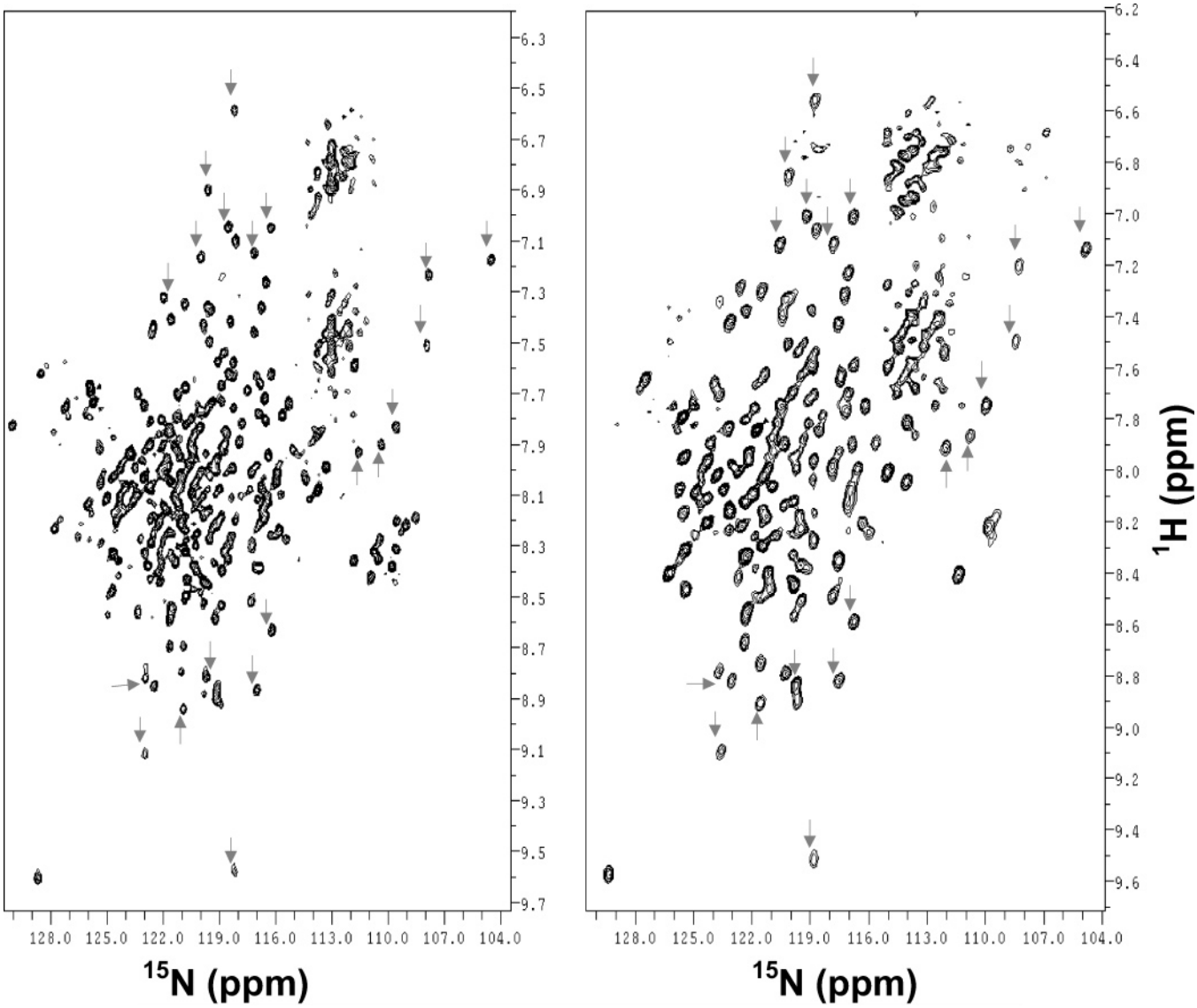

FIGURE 4: The two-dimensional TROSY ^{1}H-^{15}N HSQC spectra of ^{2}H/^{15}N/^{13}C-labeled mouse apoAI(1−240) (5 mg/mL, right panel, 180 transients) and apoAI(1−216)-P4/L3 mutant (30 mg/mL, left panel, 8 transients) in 25 mM phosphate buffer containing 25 mM NaCl, 5 mM EDTA, and 0.1 mM NaN_3, pH 7.2. Both spectra were processed using identical parameters.

240) deviates somewhat from unity at the concentration employed. The derived thermodynamic parameters, including T_m and ΔH are shown in Table 1. The thermodynamic data for all three proteins are nearly identical, suggesting that they share the same overall fold. The small deviations in T_m and enthalpies do not suggest differences in structure. The similarity in structure suggested by the calorimetric data is further confirmed by chemical denaturation using GdnHCl, as monitored by CD spectroscopy. Figure 7 shows the normalized GdnHCl denaturation curves for these three proteins, demonstrating a nearly identical $[GdnHCl]_{1/2}$ and stability shared by these three proteins, as shown in Table 2. In summary, we conclude that the monomeric apoAI(1−216) adopts an identical secondary, tertiary structure and stability as those of the wild-type apoAI(1−216).

Monomeric ApoAI(1−216) Maintains Lipid-Binding Activity of ApoAI. To test the biological function of the monomeric mutant, we mainly focused on apoAI's lipid-binding activity. Two lipid-binding assays were used, including the DMPC clearance assay and preparation of rHDL particles using POPC. The DMPC clearance assay is a common experiment to assess the lipid-binding activity of apolipoproteins, even though DMPC is not a physiologically relevant phospholipid. On the other hand, the primary function of apoAI is to assemble HDL particles; thus, an ability to generate rHDL particles with a physiologically relevant lipid, POPC, provides a different assessment of the lipid-binding activity of apoAI. Figure 8 shows the results of DMPC clearance assay at two different ratios of apoAI and DMPC and demonstrates that both apoAI(1−216) proteins display an equal ability to clear DMPC vesicles, including the initial rate and overall clearance. To confirm this result, we carried out experiments to characterize the lipid particles formed by apoAI and DMPC in the DMPC clearance assay using native gel and electron microscopy. Figure 9, left panel, shows the native gel of these DMPC particles, suggesting that the full-length mouse apoAI is able to completely transform the DMPC vesicles into discoidal HDL particles. In contrast, both apoAI-(1−216) proteins seem to display an impaired ability to generate such discoidal HDL particles with DMPC, since a significant population of lipid-free or lipid-poor apoAI is observed in the native gel. However, the discoidal HDL

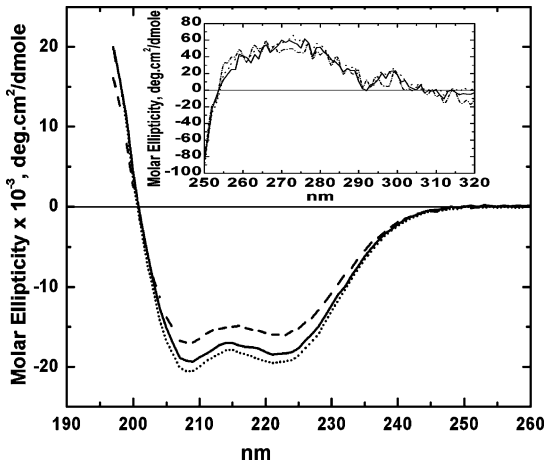

FIGURE 5: Far-UV CD spectra of apoAI(1−216)-WT, apoAI(1−216)-P4/L3 mutant, and apoAI(1−240) at 0.2 mg/mL in 50 mM sodium phosphate saline, pH 7.2. Dotted line, apoAI(1−216)-WT; solid line, apoAI(1−216)-P4/L3 mutant; dashed line, apoAI(1−240). Inset: near-UV CD spectra of these proteins. Two apoAI-(1−216) proteins, including apoAI(1−216)-WT and apoAI(1−216)-P4/L3, display nearly identical near-UV CD spectra, whereas apoAI(1−240) shows a slightly different near-UV CD spectrum.

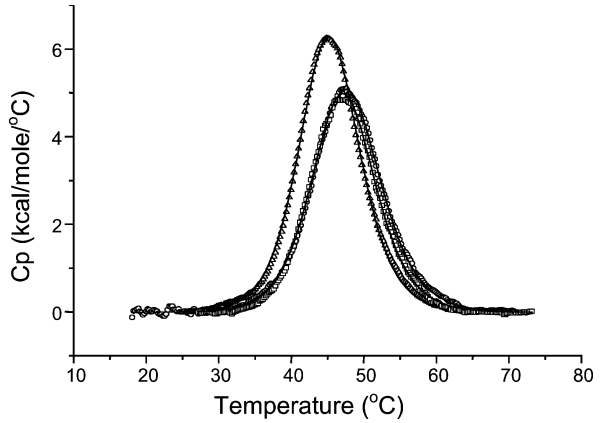

FIGURE 6: Differential scanning calorimetry of mouse apoAI proteins at pH 7.4. Raw data are shown in symbols, and fits are shown in solid lines and are superimposed for comparison. Open circles, apoAI(1−216)-WT, 0.67 mg/mL; open triangles, apoAI-(1−216)-P4/L3, 2.79 mg/mL; open squares, apoAI(1−240), 0.92 mg/mL.

Table 1: Summary of DSC Experiments of Mouse ApoAI Mutants' Thermodynamic Data Derived from a Fit to a Single, Non-Two-State Transition

protein	T_m (°C)	ΔH_c (kcal/mol)	ΔH_v (kcal/mol)	$\Delta H_v/\Delta H_c$ ratio
apoAI(1−216)-WT	47.62 (± 0.01)	62.9 (± 0.1)	66.0 (± 0.1)	1.05
apoAI(1−216)-P4/L3	45.20 (± 0.01)	69.8 (± 0.1)	72.5 (± 0.1)	1.04
apoAI(1−240)	47.15 (± 0.01)	60.0 (± 0.1)	68.1 (± 0.2)	1.14

particles formed by DMPC and apoAI(1−216)-P4/L3 or apoAI(1−216)-WT are similar to one another, though both are larger than the discoidal HDL particle formed using apoAI(1−240). This result is confirmed by electron microscopy (Figure 10), showing that the diameter of discoidal HDL formed by apoAI(1−240) is ∼10 nm, whereas these discoidal HDLs formed by apoAI(1−216) range over a much larger distribution centered at 15−20 nm. We also prepared rHDL particles with POPC (*27*). Figure 9, right panel, shows a native gel of the rHDLs prepared using POPC. It clearly illustrates that all three apoAI proteins have an ability to

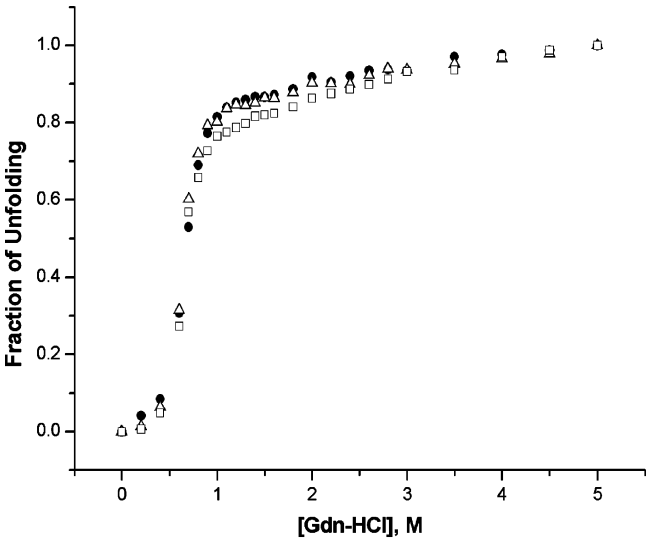

FIGURE 7: Guanidine hydrochloride denaturation of mouse apoAI-(1−216)-WT (solid circle), apoAI(1−216)-P4/L3 (open triangle), and apoAI(1−240) (open square) in 50 mM sodiumphosphate saline, pH 7.2 (0.2 mg/mL). The fraction of unfolding was plotted as a function of guanidine hydrochloride concentration.

Table 2: The Thermodynamic Data of the Proteins' Stability: Mouse ApoAI(1−216)-WT, ApoAI(1−216)-P4/L3, and ApoAI(1−240) Derived from Guanidine Hydrochloride Denaturation

sample	$\Delta G_d^{H_2O}$ (kcal/mol)	Δn (mol guan/mol)	$[GdnHCl]_{1/2}$ (M)	α-helical (%)	number of residues in α-helix
apoAI(1−216)-WT	3.73	29.12	0.67	57.6	124
apoAI(1−216)-P4/L3	3.89	30.8	0.65	55.5	120
apoAI(1−240)	4.46	34.68	0.66	48.6[a]	122

[a] Mouse apoAI(1−240) contains a 10-residue his-tag of six His and a factor Xa site.

make discoidal HDL particles. Essentially, all three mouse apoAI proteins appear to be incorporated into discs in this experiment as no lipid-free apoAI is found in Figure 9, right panel. In the native gel, mouse apoAI(1−240)/POPC particles are slightly larger than the particles formed by two mouse apoAI(1−216) proteins, but similar to the size of the particle formed using human full-length apoAI. In addition, the discoidal HDL particles formed by two mouse apoAI(1−216) proteins show an identical size. Electron microscopy confirmed this result (Figure 11), showing that all three apoAI proteins make reconstituted discoidal HDL particles with POPC in a similar shape and size distribution. Cross-linking experiments confirmed that these discoidal HDL particles contain two molecules of apoAI per particle (data not shown). In summary, we conclude that the monomeric mouse apoAI(1−216) mutant maintains the lipid-binding activity of apoAI.

DISCUSSION

A Novel Strategy for Making Monomeric, Biologically Active Protein. Two established methods for determining atomic resolution structures of proteins are X-ray crystallography and NMR spectroscopy. Both methods require that biomolecules predominantly display one oligomeric species, either a complete monomer, a complete dimer, or so forth.

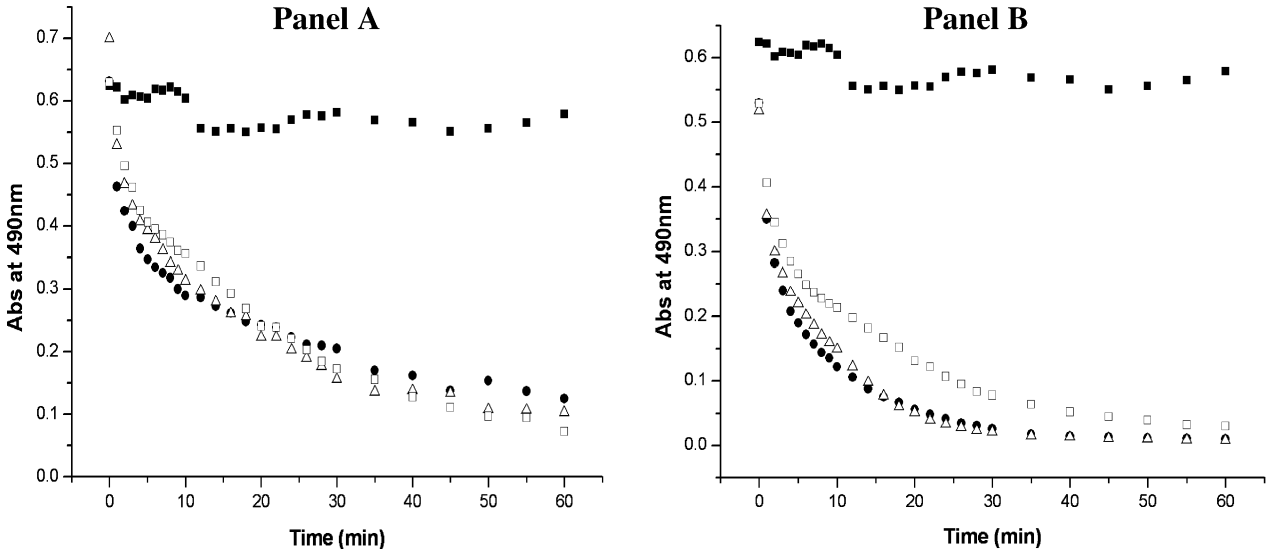

FIGURE 8: Phospholipid vesicle clearance. DMPC vesicles were incubated at 24 °C in the absence (solid square) and presence of mouse apoAI(1−216)-WT (solid circle), apoAI(1−216)-P4/L3 mutant (open triangle), and apoAI(1−240) (open square) in 20 mM Tris-HCl, pH 7.2, 250 mM NaCl, and 1 mM EDTA. Vesicle clearance as a function of time was followed by OD at 490 nm. DMPC/protein ratios (w/w) are 2.5:1 (panel A) and 1:1 (panel B).

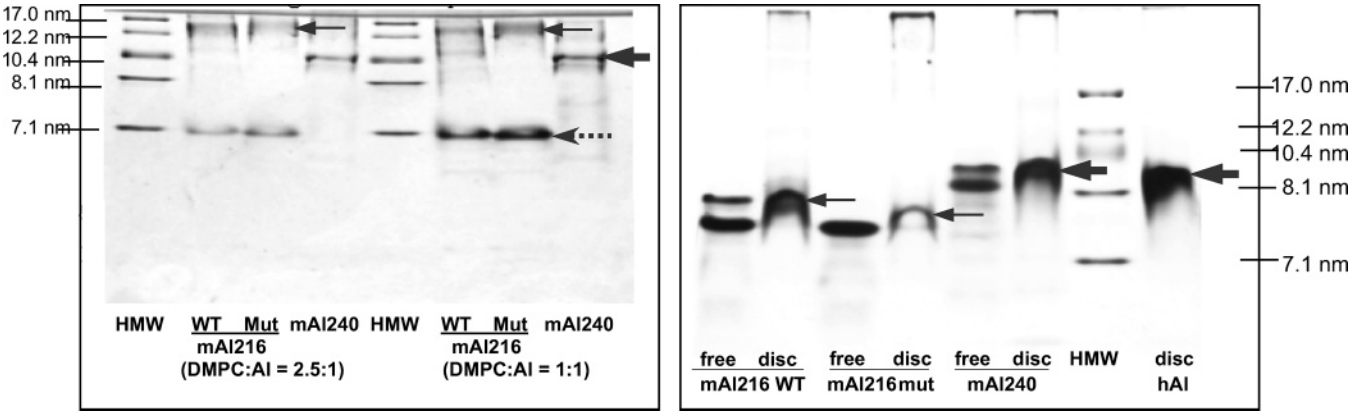

FIGURE 9: Native gels of the rHDL particles prepared using mouse apoAI(1−216)-WT, apoAI(1−216)-P4/L3, apoAI(1−240), and human apoAI (hAI) with either DMPC (left panel) or POPC (right panel) in 50 mM phosphate-buffered saline, pH 7.2. Dotted arrows, lipid-free proteins or lipid-poor particles; thin solid arrows, discoidal HDLs by mouse apoAI(1−216)/DMPC or POPC; thick solid arrows, discoidal HDLs by mouse apoAI(1−240)/DMPC or mouse apoAI(1−240)/POPC and human apoAI(1−243)/POPC.

A mixture of different oligomers prevents crystallization for X-ray crystallographic study and complicates NMR spectral analysis, since each oligomeric species produces one set of NMR signals. Indeed, many proteins display a mixture of different oligomers in solution, and aggregation is usually concentration-dependent. This is especially problematic for NMR structural determination, which generally requires a sample concentration of 0.5−1.0 mM. Even with a cryoprobe, a sample concentration of a few hundred micromolar is still required. Under such high concentrations, many proteins aggregate to form different oligomers.

Lipid-associated and membrane-associated proteins normally aggregate under a low concentration (*30*, *31*), making the structural determination of these proteins extremely difficult. To circumvent this challenge, several techniques have been developed. For example, alterations in buffer conditions, including different salts, pHs, and detergents, might reduce aggregation of some proteins (*32*). This strategy can only be used to solve the aggregation problem that is not severe and is usually time-consuming. This is a "go-and-testing" method and usually fails for lipid-associated and membrane-associated proteins. When protein-engineering is used, mutants can be prepared to mutate the critical residues that cause aggregation. The engineered mutant only forms one oligomeric species and, thus, can be used for structural determination. However, this method may possibly produce a mutant that is not biologically active or has reduced activity. In addition, this method requires previous knowledge of the critical residues that cause aggregation. Here, we report a novel strategy that allows for quick identification of these critical residues. This strategy also includes a high throughput method for quickly characterizing the oligomeric states of the mutants at different high concentrations. Among several different methods, we found that the cross-linking technique is a simple, quick experiment and many mutants can be characterized at the same time. Cross-linking experiments can also be carried out at different sample concentrations. This provides an advantage for those proteins such as apoAI, whose aggregation is concentration-dependent. Using this strategy, we have successfully prepared two monomeric, biologically active proteins, including apoAI and apoE. However, it remains to be determined if this strategy can serve as a general method of preparing monomeric, biologically active proteins.

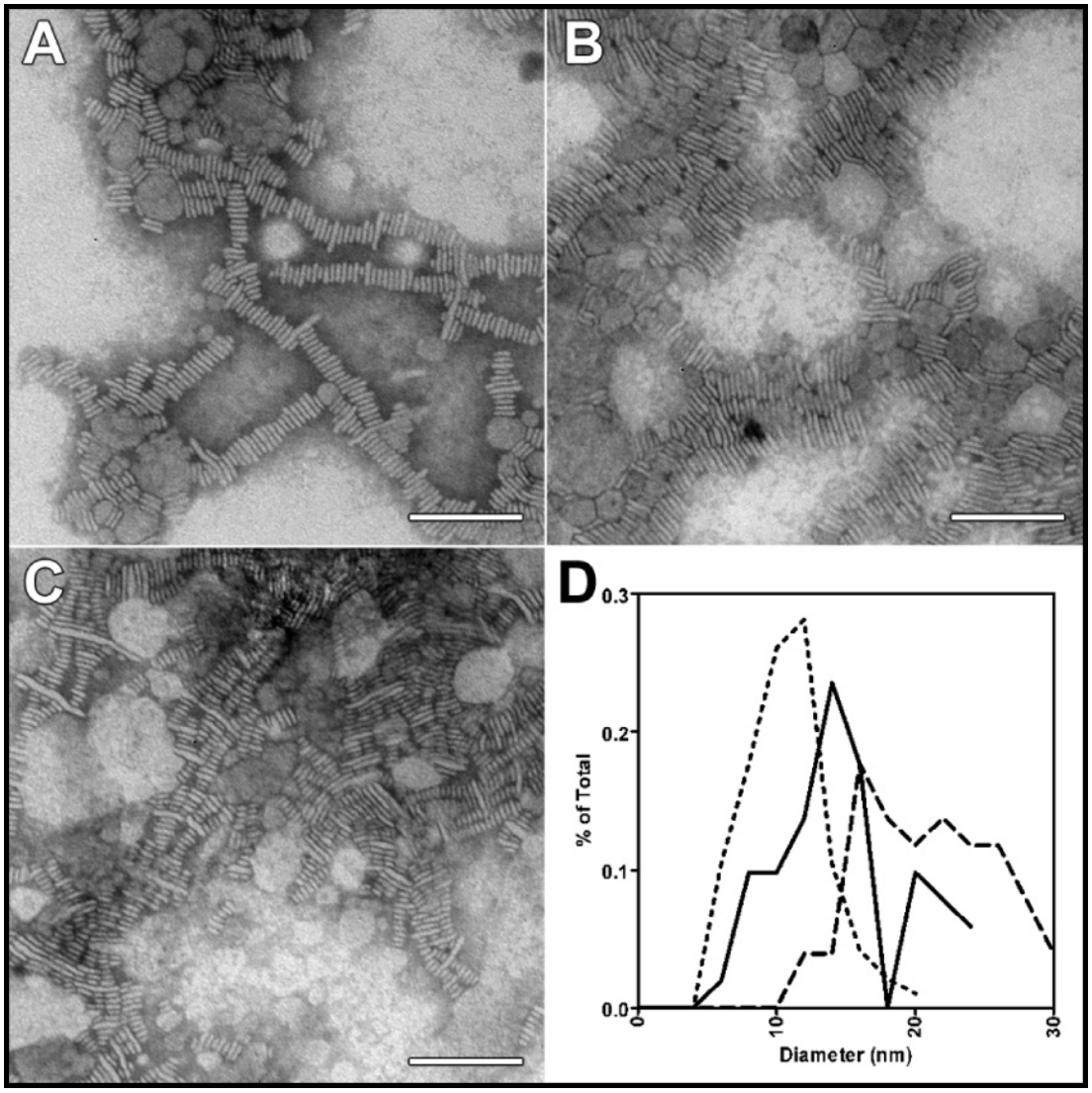

FIGURE 10: Negative stain electron microscopy of the discoidal particles formed using DMPC. (A) ApoAI(1−216)-WT; (B) apoAI(1−216)-P4/L3; and (C) apoAI(1−240). Bar = 50 nm. (D) Size distribution determined by electron microscopy of discoidal particles using apoAI(1−216)-WT (solid line), apoAI(1−216)-P4/L3 (dashed line), and apoAI(1−240) (dotted line).

A Monomeric, Biologically Active Mouse ApoAI(1−216) Mutant. Using this novel method, we prepared a monomeric apoAI(1−216) mutant and demonstrated that this monomeric mutant not only maintained the structural integrity but also displayed an equal stability as the wild-type protein. Most importantly, both the monomeric and wild-type apoAI(1−216) shared an equal ability to make rHDL particles. In Results, we reported our results using two different apoAI concentrations. To identify a monomeric mutant of apoAI that is suitable for NMR structural studies, we first carried out cross-linking experiments of the apoAI proteins at a high concentration (>5 mg/mL, Figure 2), since a monomeric apoAI mutant at a high concentration would allow us to collect high-quality NMR spectra for structural determination. Once we identify a monomeric mutant, we immediately isotope-labeled this monomeric protein and carried out NMR experiments. Indeed, this monomeric apoAI protein yielded high-quality NMR spectra as shown in Figure 4, left panel. More importantly, the spectral pattern of the monomeric apoAI(1−216) at a high concentration (30 mg/mL) is very similar to that of the wild-type apoAI(1−240) at a lower concentration (5 mg/mL) (Figure 4), suggesting that these two proteins may share an identical global fold.

To confirm this conclusion and to identify if this monomeric apoAI mutant is biologically active, we then carried out CD, GdnHCl denaturation, and lipid-binding assays at a much lower concentration of the apoAI proteins (<0.2 mg/mL), since these experiments could only be carried out at a lower concentration. We acknowledge that all of the mouse apoAI proteins at this concentration are mostly monomeric; thus, these experiments allow us to compare the structure, stability, and lipid-binding activity of the monomeric apoAI proteins, including wild-type apoAI. In fact, lipid-free apoAI concentration in vivo is lower than 0.2 mg/mL (*1*, *33*), suggesting that the monomeric form of apoAI may be the biologically active form of this protein. Our rationale is that if both the wild-type apoAI and monomeric mutant apoAI display an identical structure, stability, and lipid-binding activity, the NMR structure of the monomeric apoAI mutant obtained at a higher concentration should represent the structure of this protein in vivo. Figures 5−11 confirm that monomeric apoAI(1−216) mutant shares identical structure,

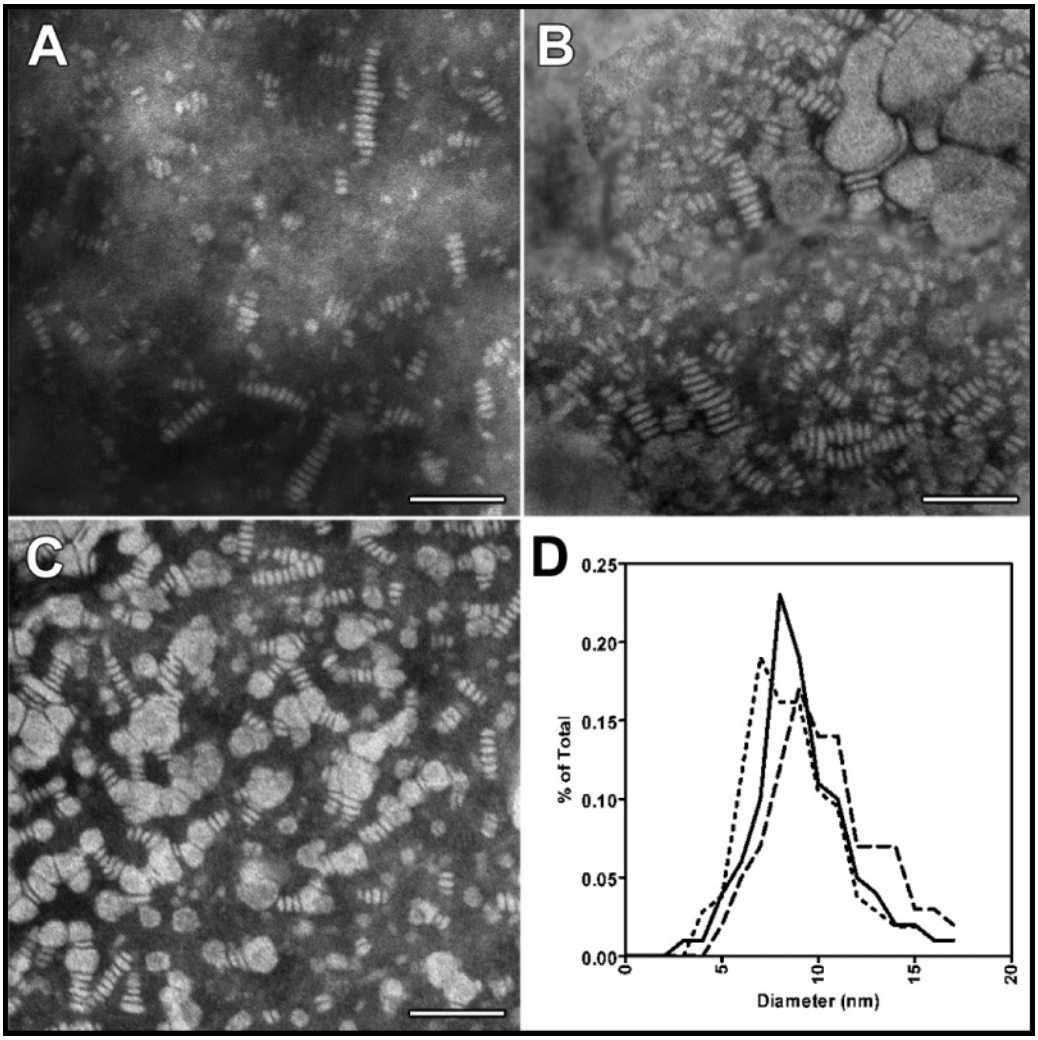

FIGURE 11: Negative stain electron microscopy of the discoidal particles formed using POPC. (A) ApoAI(1−216)-WT; (B) apoAI(1−216)-P4/L3; and (C) apoAI(1−240). Bar = 50 nm. (D) Size distribution determined by electron microscopy of discoidal particles using apoAI(1−216)-WT (solid line), apoAI(1−216)-P4/L3 (dashed line), and apoAI(1−240) (dotted line).

stability, and lipid-binding activity of wild-type apoAI protein.

We carried out DSC experiments at higher concentrations (0.7−2.8 mg/mL), since these are the concentrations at which the mouse proteins were predominantly monomeric as evidenced by cross-linking experiments. The DSC data (Figure 6 and Table 1) also indicate a similar structural cooperativity for all mouse apoAI proteins. Relative to our NMR experiments, it is important that the DSC data is consistent with a single-folded structure. Alternatively, DSC data of a C-terminal truncation mutant of human apoAI, apoAI(1−187), provided the same result (*34*). Small differences in T_m and enthalpies were observed (Table 1). In particular, apoAI(1−216)-P4/L3 shows a somewhat lower T_m and higher enthalpy than both apoAI(1−216)-WT and apoAI(1−240). While these differences are very small, they are not surprising, given the mutations made. Nevertheless, such a small difference in T_m and enthalpy between the wild-type and the monomeric apoAI suggests that the mutations introduced do not significantly change the overall stability of apoAI.

ApoAI also plays a critical role in HDL maturation, which includes the LCAT activation and binding to the HDL receptor, SR-BI, for selective lipid-uptake by the liver. However, these activities of apoAI depend on the lipid-binding activity. Previous results indicated that a mutant that displayed an identical lipid-binding activity with the mutating sites outside of the domains that were responsible for LCAT activation or SR-BI binding displayed an equal ability to activate LCAT and SR-BI binding (*35*, *36*). Indeed, the mutation sites of the monomeric apoAI mutant are either in the C-terminal region or in loop 3, which is outside of the LCAT activation domain and SR-BI-binding domain. Thus, we suggest that the monomeric apoAI(1−216) mutant is biologically active. Such a biologically active apoAI mutant may serve as the representative apoAI for structural studies using either X-ray crystallography or NMR techniques. We demonstrated that we have collected high-quality NMR spectra of this monomeric apoAI, allowing us to determine the high-resolution NMR structure of lipid-free apoAI (Figure 4, left panel).

The monomeric, biologically active apoAI mutant replaces six residues in two separate regions. The selection of the mutations is not random but based on the rationale that utilizes sequence comparisons and previous knowledge of structure−function relationship of apoAI. We prepared helix wheel diagrams that allowed us to quickly identify three Thr residues that were located in the hydrophilic surface.

Replacing these three Thr residues with conservative residue Ser immediately reduced aggregation of apoAI(1−206). In fact, helix wheel diagrams also showed that several other hydrophobic residues were also located in the hydrophilic surface of the helix, such as T153/T160 in helix 6, A174/A178 in helix 7, and T221/T224 in helix 10 (Figure 3). We took advantage of the close proximity of these residues in apoAI primary sequence and designed primers in which one primer contained several mutations. For example, primer 4 contained three mutations in helix 8: T191S/T195S/T199S. In this case, only six primers were made which covered all 12 mutations; thus, all mutations were achieved very quickly. These mutations were characterized, and no major changes of the oligomeric states were observed except for the P4 mutant, suggesting that helix 8 was one of the major sites that caused apoAI aggregation. Interestingly, previous evidence also indicated that this region of apoAI is important for apoAI's aggregation property (*4*).

Previous ultracentrifugation data also indicated that lipid-free apoAI might exist as a rodlike structure with a significant population (*5*). Only two situations are possible for a rodlike structure: a single long helix or two helix-bundles aggregated together using the "head-to-head" manner. We anticipate that a single long helix of apoAI is nearly impossible, since this structure does not fit into the published experimental data. We hypothesized that the rodlike structure is an oligomer of two helix-bundles with a "head-to-head" aggregation. In this case, the loops that connect helices in the apoAI helix-bundle provide the aggregation sites. Indeed, sequence analysis of the loops in apoAI indicated that the residues in these loops are mostly bulky hydrophobic residues. This is quite different from human apoE N-terminal domain and insect apolipoprotein, apoLp-III, whose structures are known to be monomeric (*37*−*40*). On the basis of this analysis, we prepared four loop primers which covered loops 1, 3, 4, and 5. The loop 1 ($L_{63}GPLT_{67}$) was mutated to $L_{63}GPSS_{67}$. The loop 3 ($V_{118}APL_{121}$) was mutated to $A_{118}SPQ_{121}$. The loop 4 ($L_{140}SPVA_{144}$) was mutated to $L_{140}SPSS_{144}$, and loop 5 ($L_{162}APH_{165}$) was mutated to $S_{162}SPH_{165}$. The loops 2 and 6 are quite hydrophilic; thus, no mutations were made for these two loops, whereas apoAI(1−216) only contained half of the loop 7, which is hydrophilic. Characterizations of these loop mutants indicated that apoAI(1−216)-P4/L3, a mutant that contained primer 4 and loop 3 mutations, displayed nearly 90% monomer with <10% dimer at 8 mg/mL.

Self-Association Is Not Essential for ApoAI's Structure and Function. Previous data indicated that the C-terminal domain of apoAI is responsible for the aggregation property and lipid-binding activity (*1*, *2*). This raises the question whether the aggregation property is correlated with the lipid-binding activity. This question remains unanswered for all members of human exchangeable apolipoprotein family, since they share a common aggregation property and lipid-binding activity. For example, it was hypothesized that the LDL receptor binding activity of apoE is correlated with the tetramerization property of this protein (*41*). Our results demonstrated that the self-association property of apoAI was not essential for its structure and function. The mutant that diminishes the aggregation property of apoAI maintains its structure and stability and displays an identical ability to make rHDL particles. The main function of apoAI is to assemble HDL particles in the reverse cholesterol transport pathway. The ability to make rHDL particles with physiological phospholipid, POPC, is proposed to represent the lipoprotein-binding activity of this protein. Our results demonstrate that the critical residues for apoAI aggregation are not the same residues that are responsible for its lipid-binding activity. Recently, we also prepared a monomeric, biologically active apoE C-terminal domain (*18*) and full-length apoE using the same strategy (manuscript in preparation). Since apoAI and apoE are the two main members of exchangeable apolipoproteins, a general conclusion may be drawn for the apolipoprotein family that the self-association property may not be essential for their lipoprotein-binding activity.

We noticed the differences between the rHDL prepared by apoAI(1−216) and the particles prepared by full-length apoAI. First, apoAI(1−216) could not make complete discoidal HDL particles with DMPC. In contrast, full-length mouse apoAI was able to make complete discoidal HDL with DMPC. The particle sizes of the rHDL prepared using these two apoAI proteins are slightly different. Nevertheless, both the C-terminal 24-residue truncation mutant and full-length apoAI are able to make rHDL particles with DMPC. The difference displayed here indicates that the C-terminal 24-residues provide extra lipid-binding capability for this protein. When POPC is used, both the C-terminal truncation mutants and full-length apoAI displayed an ability to convert nearly 100% lipid-free apoAI into the rHDL particles, suggesting that these proteins displayed an equal ability to make reconstituted discoidal HDL particles using POPC. Since the POPC is a physiological phospholipid whereas DMPC is not, we suggest that apoAI(1−216) maintains the integrity of apoAI's lipid-binding activity. However, our data also suggests that the C-terminal 24-residues play an additional role in promoting lipid-binding activity.

ApoAI(1−216) Structure May Represent Lipid-Free Mouse ApoAI Structure. To date, no high-resolution structure of lipid-free full-length apoAI is available. Our monomeric apoAI mutant lacks the C-terminal 24-residues. One question remains to be addressed: whether the structure of this apoAI C-terminal truncation mutant represents the lipid-free structure of full-length apoAI. To answer this question, we prepared triple-labeled, full-length mouse apoAI with $^{2}H/^{13}C/^{15}N$ and collected TROSY ^{1}H-^{15}N HSQC NMR spectrum at a low concentration (5 mg/mL). Because of significant aggregation of the full-length apoAI, we could not obtain high-quality NMR spectra, since some of the cross-peaks were missing due to a slower tumbling of the larger oligomers (Figure 4, right panel). However, the overall spectral pattern of full-length mouse apoAI is similar to the spectral pattern of the monomeric apoAI(1−216) as highlighted by arrows (Figure 4), suggesting that these two proteins may adopt a similar tertiary structure. Previous published data also indicated that deletion of residues 187−243 in human apoAI did not dramatically alter the overall structure of this protein in the lipid-free state (*5*). Therefore, the NMR structure of the monomeric mouse apoAI may represent the structure of this protein in its lipid-free state.

The NMR spectrum of the monomeric apoAI suggests that this protein may adopt a helix-bundle structure in the lipid-free state due to a large chemical shift dispersion of the backbone NH (∼3.0 ppm). The large chemical shift dispersion suggests a potential helix−helix interaction, which

separates the chemical shifts of the residues in the helices. Usually, the amide proton chemical shift dispersion of a single helix is very small, ranging between 0.7 and 1.0 ppm, since all the amide protons on this helix are essentially located in the same chemical environment. On the other hand, a helix-bundle contains helix−helix interactions which are usually involved in hydrophobic residues. These helix−helix interactions make the chemical environment of amide proton different, thus, causing the larger chemical shift dispersion. This conclusion was confirmed by the chemical shift of the methyl protons. We observe several methyl protons at the chemical shift between −1.0 and 0.0 ppm (data not shown). Such a small chemical shift of methyl protons indicates helix−helix interactions in apoAI, suggesting that lipid-free apoAI may adopt a helix-bundle structure. A helix-bundle structure of lipid-free apoAI is completely different from the "belt model" of apoAI structure that is proposed for apoAI on discoidal particles (*42*). It is also different from the X-ray structure of the apoAI(44−243) mutant (*11*). However, this helix-bundle structure agrees with the recent published results using either ultracentrifugation (*5*), fluorescence techniques (*34*, *43*), or cross-linking/mass spectrometry (*44*). Nevertheless, the monomeric, biologically active apoAI(1−216) provides us with an opportunity to solve the lipid-free apoAI structure, and we are currently working on this aspect.

ACKNOWLEDGMENT

The authors thank Dr. Qianqian Li for her help in preparation of several DNA constructs used in this project and for critical reading of the manuscript and helpful discussion and Dr. Irina Protasevich for helpful discussion.

REFERENCES

1. Brouillette, C. G., Anantharamaiah, G. M., Engler, J. A., and Borhani, D. W. (2001) Structural models of human apolipoprotein A-I: a critical analysis and review, *Biochim. Biophys. Acta 1531*, 4−46.
2. Frank, P. G., and Marcel, Y. L. (2000) Apolipoprotein A-I: structure−function relationships, *J. Lipid Res. 41*, 853−872.
3. Vitello, L. B., and Scanu, A. M. (1976) Studies on human serum high-density lipoproteins. Self-association of apolipoprotein A-I in aqueous solutions, *J. Biol. Chem. 251*, 1131−1136.
4. Laccotripe, M., Makrides, S. C., Jonas, A., and Zannis, V. I. (1997) The carboxyl-terminal hydrophobic residues of apolipoprotein A-I affect its rate of phospholipid binding and its association with high-density lipoprotein, *J. Biol. Chem. 272*, 17511−17522.
5. Rogers, D. P., Roberts, L. M., Lebowitz, J., Engler, J. A., and Brouillette, C. G. (1998) Structural analysis of apolipoprotein AI: effects of amino- and carboxy-terminal deletions on the lipid-free structure, *Biochemistry 37*, 945−955.
6. Marcel, Y. L., and Kiss, R. S. (2003) Structure−function relationships of apolipoprotein AI: a flexible protein with dynamic lipid associations., *Curr. Opin. Lipidol. 14*, 151−157.
7. Barrans, A., Jaspard, B., Barbaras, R., Chap, H., Perret, B., and Collet, X. (1996) Preβ HDL: structure and metabolism, *Biochim. Biophys. Acta 1300*, 73−85.
8. Smith, J. D., Le Goff, W., Settle, M., Brubaker, G., Waelde, C., Horwitz, A., and Oda, M. N. (2004) ABCA1 mediates concurrent cholesterol and phospholipid efflux to apoAI, *J. Lipid. Res. 45*, 635−644.
9. Yokoyama, S. (2005) Assembly of high-density lipoprotein by the ABCA1/apolipoprotein pathway, *Curr. Opin. Lipidol. 16*, 269−279.
10. Navab, M., Hama, S. Y., Hough, G. P., Hedrick, C. C., Sorenson, R., La Du, B. N., Kobashigawa, J. A., Fonarow, G. C., Berliner, J. A., Laks, H., and Fogelman, A. M. (1998) High-density associated enzymes: their role in vascular biology, *Curr. Opin. Lipidol. 9*, 449−456.
11. Borhani, D. W., Rogers, D. P., Engler, J. A., and Brouillette, C. G. (1997) Crystal structure of truncated human apolipoprotein AI suggests a lipid-bound conformation, *Proc. Natl. Acad. Sci. U.S.A. 94*, 12291−12296.
12. Borhani, D. W., Engler, J. A., and Brouillette, C. G. (1999) Crystallization of truncated human apolipoprotein A-I in a novel conformation, *Acta Crystallogr., Sect. D: Biol. Crystallogr. 55*, 1578−1583.
13. Okon, M., Frank, P. G., Marcel, Y. L., and Cushley, R. J. (2001) Secondary structure of human apolipoprotein A-I(1−186) in lipid-mimetic solution, *FEBS Lett. 487*, 390−396.
14. Okon, M., Frank, P. G., Marcel, Y. L., and Cushley, R. J. (2002) Heteronuclear NMR studies of human serum apolipoprotein AI. Part I. Seconday structure in lipid-mimetic solution, *FEBS lett. 517*, 139−143.
15. Li, H., Lyles, D. S., Thomas, M. J., Pan, W., and Sorci-Thomas, M. G. (2000) Structural determination of lipid-bound ApoA-I using fluorescence resonance energy transfer, *J. Biol. Chem. 275*, 37048−37054.
16. Davidson, W. S., and Hilliard, G. M. (2003) The spatial organization of apolipoprotien AI on the edge of discoidal high-density lipoprotein particles, *J. Biol. Chem. 278*, 27199−27207.
17. Koppaka, V., Silvestro, L., Engler, J. A., Brouillette, C. G., and Axelsen, P. H. (1999) The structure of human lipoprotein A-I. Evidence for the "belt" model, *J. Biol. Chem. 274*, 14541−14544.
18. Fan, D., Li, Q., Korando, L., Jerome, W. G., and Wang, J. (2004) A monomeric human apolipoprotein E carboxyl-terminal domain, *Biochemistry. 43*, 5055−5064.
19. Aggerbeck, L. P., Wetterau, J. R., Weisgraber, K. H., Wu, C. S., and Lindgren, F. T. (1988) Human apolipoprotein E3 in aqueous solution. II. Properties of the amino- and carboxyl-terminal domains, *J. Biol. Chem. 263*, 6249−6258.
20. Reschly, E. J., Sorci-Thomas, M. G., Davidson, W. S., Meredith, S. C., Reardon, C. A., and Getz, G. S. (2002) Apolipoprotein A-I α-helices 7 and 8 modulate high-density lipoprotein subclass distribution, *J. Biol. Chem. 277*, 9645−9654.
21. Pace, C. (1986) Determination and analysis of urea and guanidine hydrochloride denaturation curves, *Methods Enzymol. 131*, 266−280.
22. Markwell, M. A., Haas, S. M., Bieber, L. L., and Tolbert, N. E. (1978) A modification of the Lowry procedure to simplify protein determination in membrane and lipoprotein samples, *Anal. Biochem. 87*, 206−210.
23. Delaglio, F., Grzesiek, S., Vuister, G. W., Zhu, G., Pfeifer, J., and Bax, A. (1995) NMRPipe: a multidimensional spectral processing system based on UNIX pipes, *J. Biomol. NMR. 6*, 277−293.
24. Garrett, D. S., Powers, R., Gronenborn, A. M., and Clore, G. M. (1991) A common sense approach to peak picking two-, three- and four-dimensional spectra using automatic computer analysis of contour diagrams, *J. Magn. Reson. 95*, 214−220.
25. MacDonald, R. C., MacDonald, R. I., Menco, B. P., Takeshita, K., Subbarao, N. K., and Hu, L. R. (1991) Small-volume extrusion apparatus for preparation of large, unilamellar vesicles, *Biochim. Biophys. Acta 1061*, 297−303.
26. Surewicz, W. K., Epand, R. M., Pownall, H. J., and Hui, S. W. (1986) Human apolipoprotein A-I forms thermally stable complexes with anionic but not with zwitterionic phospholipids, *J. Biol. Chem. 261*, 16191−16197.
27. Jonas, A. (1986) Reconstitution of high-density lipoproteins, *Methods Enzymol. 128*, 553−582.
28. Jonas, A., Kezdy, K. E., and Wald, J. H. (1989) Defined apolipoprotein A-I conformations in reconstituted high-density lipoprotein discs, *J. Biol. Chem. 264*, 4818−4824.
29. Sparks, D. S., Frank, P. G., Braschi, S., Neville, T. A. M., and Marcel, Y. L. (1999) Effect of apolipoprotein AI lipidation on the formation and function of pre-β and α-migrating LpA-I particles, *Biochemistry 38*, 1727−1735.
30. Westerlund, J. A., and Weisgraber, K. H. (1993) Discrete carboxyl-terminal segments of apolipoprotein E mediate lipoprotein association and protein oligomerization, *J. Biol. Chem. 268*, 15745−15750.
31. Tessier, P. M., and Lenhoff, A. M. (2003) Measurements of protein self-association as a guide to crystallization, *Curr. Opin. Biotechnol. 14*, 512−516.
32. Cudney, R. (1994) Screening and optimization strategies for macromolecular crystal growth, *Acta Crystallogr., Sect. D: Biol. Crystallogr. 50*, 414−423.

33. Naito, H. K. (1986) The clinical significance of apolipoprotein measurements., *J. Clin. Immunol. 9*, 11−20.
34. Brouillette, C. G., Dong, W., Yang, Z. W., Ray, M. J., Protasevich, I. I., Cheung, H. C., and Engler, J. A. (2005) Förster resonance energy transfer measurements are consistent with a helical bundle model for lipid-free apolipoprotein A-I, *Biochemistry*, submitted for publication.
35. Thuahnai, S. T., Lund-Katz, S., Anantharamaiah, G. M., Williams, D. L., and Phillips, M. C. (2003) A quantitative analysis of apolipoprotein binding to SR-BI: multiple binding sites for lipid-free and lipid-associated apolipoproteins, *J. Lipid. Res. 44*, 1132−1142.
36. Sviridov, D., Hoang, A., Sawyer, W. H., and Fidge, N. H. (2000) Identification of a sequence of apolipoprotein A-I associated with the activation of Lecithin:Cholesterol acyltransferase, *J. Biol. Chem. 275*, 19707−19712.
37. Wilson, C., Wardell, M. R., Weisgraber, K. H., Mahley, R. W., and Agard, D. A. (1991) Three-dimensional structure of the LDL receptor-binding domain of human apolipoprotein E, *Science 252*, 1817−1822.
38. Breiter, D. R., Kanost, M. R., Benning, M. M., Wesenberg, G., Law, J. H., Wells, M. A., Rayment, I., and Holden, H. M. (1991) Molecular structure of an apolipoprotein determined at 2.5-Å resolution, *Biochemistry 30*, 603−608.
39. Fan, D., Zheng, Y., Yang, D., and Wang, J. (2003) NMR solution structure and dynamics of an exchangeable apolipoprotein, *Locusta migratoria* apolipophorin III, *J. Biol. Chem. 278*, 21212−21220.
40. Wang, J., Sykes, B. D., and Ryan, R. O. (2002) Structural basis for the conformational adaptability of apolipophorin III, a helix-bundle exchangeable apolipoprotein, *Proc. Natl. Acad. Sci. U.S.A. 99*, 1188−1193.
41. Weisgraber, K. (1994) Apolipoprotein E: structure−function relationships, *Adv. Protein Chem. 45*, 249−302.
42. Segrest, J. P., Jones, M. K., Klon, A. E., Sheldahl, C. J., Hellinger, M., De Loof, H., and Harvey, S. C. (1999) A detailed molecular belt model for apolipoprotein A-I in discoidal high-density lipoprotein, *J. Biol. Chem. 274*, 31755−31758.
43. Davidson, W. S., Arnvig-McGuire, K., Kennedy, A., Kosman, J., Hazlett, T. L., and Jonas, A. (1999) Structural organization of the N-terminal domain of apolipoprotein A-I: studies of tryptophan mutants, *Biochemistry 38*, 14387−14395.
44. Silva, R. A., Hilliard, G. M., Fang, J., Macha, S., and Davidson, W. S. (2005) A three-dimensional molecular model of lipid-free apolipoprotein A-I determined by cross-linking/mass spectrometry and sequence threading, *Biochemistry 44*, 2759−2769.

BI0508385